Knee Joint Misalignment in Exoskeletons for the Lower Extremities: Effects on User's Gait

Damiano Zanotto, *Member, IEEE*, Yasuhiro Akiyama, Paul Stegall, *Student Member, IEEE*, and Sunil K. Agrawal, *Member, IEEE*

***Abstract*—Due to the complexity of the human musculoskeletal system and intra/intersubjects variability, powered exoskeletons are prone to human–robot misalignments. These induce undesired interaction forces that may jeopardize safe operation. Uncompensated inertia of the robotic links also generates spurious interaction forces. Current design approaches to compensate for misalignments rely on the use of auxiliary passive degrees of freedom that unavoidably increase robot inertia, which potentially affects their effectiveness in reducing undesired interaction forces. Assessing the relative impact of misalignment and robot inertia on the wearer can, therefore, provide useful insights on how to improve the effectiveness of such approaches, especially in those situations where the dynamics of the movement are quasi-periodic and, therefore, predictable such as in gait. In this paper, we studied the effects of knee joint misalignments on the wearer's gait, by using a treadmill-based exoskeleton developed by our group, the ALEX II. Knee joint misalignments were purposely introduced by adjusting the mismatch between the length of the robot thigh and that of the human thigh. The amount of robot inertia reflected to the user was adjusted through control. Results evidenced that knee misalignment significantly changes human–robot interaction forces, especially at the thigh interface, and this effect can be attenuated by actively compensating for robot inertia. Misalignments caused by an excessively long robot thigh are less critical than misalignments of equal magnitude deriving from an excessively short robot thigh.**

***Index Terms*—Active leg exoskeleton (ALEX II), force control, human–robot misalignment, rehabilitation robotics.**

I. Introduction

MANY powered exoskeletons have been proposed in recent years, both for the upper and for the lower extremities. Their field of application is broad, ranging from motor rehabilitation [1] or assistance [2] of impaired users, to performance augmentation [3]. In all the cases, these machines are designed to mimic the kinematics of human joints.

The human skeletal system includes bones, cartilage, and ligaments; these form complex kinematic chains whose behavior can be approximated, to some extent, by mechanical joints commonly used in robotics. A relevant example is the human knee; the geometry of femoral and tibial condyles and the action of the cruciate and collateral tendons restrict the relative movements of tibia and femur in flexion and extension [4], with limited medial/lateral rotations ($<9\ ^\circ$) occurring only near full extension [5]. Knee flexion/extension is often modeled by a hinge joint, even though it is actually the result of combined rolling and gliding, with the instant center of rotation moving inside a circle of diameter ≈ 20 mm centered on the lateral femoral epicondyle [6]–[8].

Intra- and inter-subject differences also affect the accuracy of kinematic models of the human limbs (e.g., deformation of cartilages and soft tissues surrounding the bones, differences in size and shape of bones among different subjects, etc.); therefore, discrepancies between the two kinematic chains—the robotic and the human—are almost unavoidable. If the physical connections between robot and human chains were perfectly rigid, kinematic incompatibility between the two systems would prevent motion. Physical robot–human interface, however, often consists of compliant orthoses, and the tissues surrounding bones and cartilages (epithelial, muscular, and nervous) can withstand large deformations [9]. This distributed compliance accommodates kinematic discrepancies, making it possible for exoskeletons to be worn and effectively operated by the user.

Joint misalignments generate undesired interaction forces onto the human limbs, which might jeopardize safe human–robot interaction; these are hard to quantify, unless proper force transducers are attached at each interface with the user. For this reason, research efforts have been conducted over the past few years, which focus on the problem of exoskeleton misalignments [10], [11]. Some of these works [9], [12] have developed systematic design methodologies to compensate for misalignments; thus, reducing undesired/uncontrolled interaction forces. To date, most of the design approaches proposed to tackle the problem of human/robot misalignment have focused on the human arm, whereas a little attention has been devoted to misalignment in exoskeletons for the lower extremities. Applying these theoretical approaches often result in additional design efforts and more complex, bulky, and expensive solutions compared with simpler designs that assume ideal alignment. Auxiliary passive degrees of freedom (DOF) have to be included in the basic robot structure [9], [11], [12], which might increase significantly the mechanical impedance of the machine (i.e., the combined effects of its inertia, friction, and weight), especially if they are located on a distal joint. While gravity and friction are relatively simple to compensate by control, masking robot inertia is a challenging task [13]. Such uncompensated mechanical impedance generates undesired interaction forces onto the user [14]. Therefore, in order for these misalignment compensation approaches not to affect the user's safety and comfort or the

Manuscript received January 22, 2015; revised June 16, 2015; accepted June 22, 2015. Date of publication August 4, 2015; date of current version August 4, 2015. This paper was recommended for publication by Associate Editor J. Dai and Editor B. J. Nelson upon evaluation of the reviewers' comments.

D. Zanotto, P. Stegall, and S. K. Agrawal are with the Robotics and Rehabilitation Laboratory, Columbia University, New York, NY 10027 USA (e-mail: damiano.zanotto@columbia.edu; stegallp@gmail.com; sunil.agrawal@columbia.edu).

Y. Akiyama is with the Department of Mechanical Science and Engineering, Nagoya University, Nagoya 467-8601, Japan (e-mail: akiyama-yasuhiro@mech.nagoya-u.ac.jp).

Color versions of one or more of the figures in this paper are available online at http://ieeexplore.ieee.org.

Digital Object Identifier 10.1109/TRO.2015.2450414

device accuracy in rendering desired forces, the tradeoff between spurious interaction forces due to misalignment and those due to uncompensated inertia of the robotic links should be studied. For devices designed to assist the gait, this may be done in a reliable way, since the dynamics involved in steady-state walking are approximately periodic, and, therefore, predictable. At faster walking speeds, the lower extremities produce higher angular velocities and accelerations [15]. These affect the contribution of robot inertia—and, possibly, its interaction with joint misalignments, suggesting that walking speed must also be included in the analysis.

As a first step toward this direction, this study investigates: 1) how the introduction of a small controlled knee misalignment in an exoskeleton for the lower extremities affects undesired human/robot interaction forces, and how these forces eventually affect kinematics and timing of the gait; 2) how the impact of misalignment on the aforementioned biomechanical variables compares with that of uncompensated inertia of the robotic links, and what interactions may occur between the two factors; 3) how the effect of these factors varies as the walking speed changes.

To answer these questions, we conducted an experiment on a small group of healthy subjects who walked in the active leg exoskeleton (ALEX II) under different configurations of the robot, with the device controlled in a *transparent mode* (i.e., nil desired interaction force). We intentionally introduced a small misalignment at the knee joint by modifying the exoskeleton adjustments, and observed the effect of these misalignments on the wearer at moderate and fast walking speeds, with and without compensation of the robot inertia. With the robot controlled in a transparent mode, any force/torques measured at the physical interfaces with the user yielded direct estimates of the undesired human–robot interaction forces.

II. Methods

A. Experimental Setup

ALEX II is a unilateral treadmill-based exoskeleton for the lower extremities developed by our group [16] [see Fig. 1(a)]. The device features two active DOFs at the leg (hip and knee flexion/extension) and four passive DOFs at the trunk (horizontal and vertical translations and vertical rotation). No auxiliary mechanism is currently installed in the robot to compensate for joint misalignment. Human–robot interactions are sensed by two six-axis sensors[1] mounted at the interfaces with the user: the thigh and the shank orthoses. Torques exerted by the gear motors are measured at the powered joints by means of single-axis sensors. Details on the design and control of ALEX II can be found in [17] and [18]; the use of this device in robot-assisted gait training of stroke survivors has been recently reported in [19].

In this experiment, ALEX II was attached to the users' left leg and the length of the telescopic thigh link was modified across the walking sessions to induce controlled misalignments on the knee joint. In a recent study, we experimentally verified that by controlling the interaction error as opposed to the torque output by the gear motors (i.e., noncollocated actuation and force sensing, see Section II-C, [20], [21]), a significant fraction

[1]ATI Industrial Automation, Apex, NC, USA.

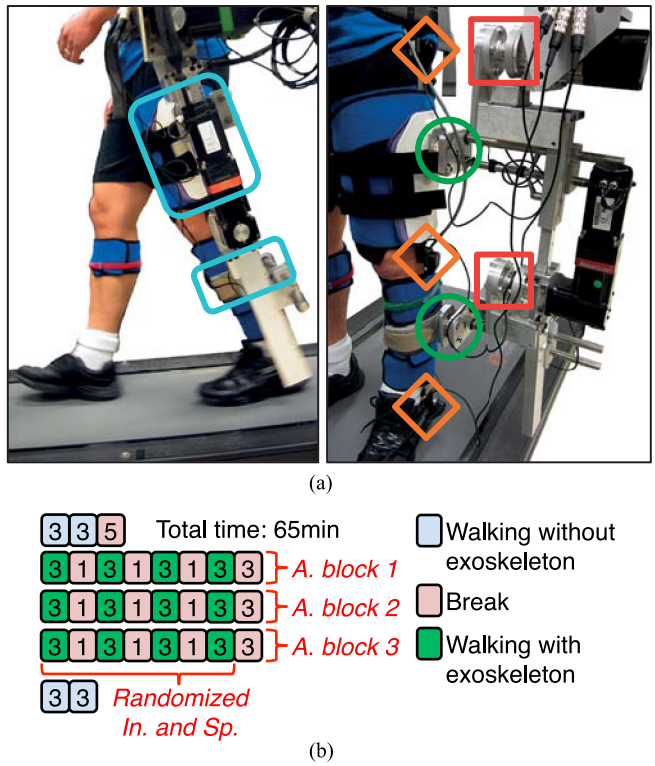

Fig. 1. (a) Subject wearing the ALEX II. Thigh and shank orthoses are indicated by cyan rounded rectangles, force/torque sensors and single-axis torque sensors are highlighted by green circles and red squares, respectively. Orange diamonds mark the locations of the hip, knee, and ankle goniometers. (b) Experimental protocol: *In*= Inertia, *Sp*= Speed, *A*= Alignment.

of the interaction forces due to robot inertia is masked from the user [14]. Building upon this observation, in this study, we simulated two conditions: partially compensated robot inertia (*CI*) versus uncompensated robot inertia (*UI*).

B. Subjects and Experimental Protocol

Nine healthy adult individuals (eight male, one female, age 27.9 ± 4.0 years, height 1.75 ± 0.06 m, weight 73.8 ± 13.6 kg) volunteered in this experiment, which consisted of a single visit to the laboratory. All subjects were right-leg dominant and had no musculoskeletal or neurological problems. Ethical approval was obtained by the local Institutional Review Board, and each subject gave informed consent before participating in the study.

The same investigator was responsible for measuring subject's biometric data relevant to the experiment. The positions of the greater trochanter, lateral femoral epicondyle, and lateral malleolus on the subject's left leg were marked on the skin, and the lengths of the human thigh and shank segments were ascertained based on distances between these landmarks, rounded to the nearest half centimeter. For each subject, three lengths of the robot thigh were tested: *short*, *ideal,* and *long*. The measured length of the subject's thigh was taken as the *ideal* length of the robot thigh, whereas the *short* and *long* lengths were defined based on the ideal length by subtracting and adding 20 mm, respectively. This value was chosen to ensure that knee misalignments induced by the *short* and *long* thigh lengths were substantially larger than any *uncontrolled* misalignment that

could arise—even with the *ideal* length—due to the nonperfect fitting of the robotic leg on the human. In practice, the misalignments imposed in this study overestimate those that can be reasonably expected in existing lower extremities power exoskeletons.

To measure flexion/extension angles of the human leg, potentiometric goniometers[2] were aligned to subject's hip, knee, and ankle joints by means of Velcro straps [see Fig. 1(a)]. Prior to the actual recording, subjects familiarized with walking in the robot for approximately 5 min [see Fig. 1(b)]. If necessary, the adjustments of the robotic leg (except for the lengths of the thigh and shank links) were further tuned to improve the wearer's comfort. Then, subjects walked in the treadmill at *slow* (0.8 m/s) and *fast* (1.1 m/s) speeds without the robot (free-walking trials) for 3 min at each speed. Subsequently, they underwent a set of 12 3-min trials [see Fig. 1(b)], each corresponding to a different combination of robot inertia (factor *In*, with to levels: *CI*—Compensated Inertia and *UI*—Uncompensated Inertia), walking speed (factor *Sp*, with two levels: *slow* speed and *fast* speed) and knee joint alignment (factor A, with three levels: *short* alignment, *ideal* alignment, *long* alignment). Speed values were chosen based on data from previous experiments with ALEX II [17], [18]. Changing robot alignment required the subject to doff the device as the experimenter adjusted the length of the thigh link to the desired value. In ALEX II, this operation takes 2–3 min, and is, therefore, more time consuming than changing the inertia compensation mode or the treadmill speed. To simplify the experimental protocol, the order of the trials was, therefore, arranged by alignment, and the factors *In* and *Sp* were randomized within each alignment block. The order of the alignment blocks was randomized across participants. Breaks within a block lasted 1 min, those between blocks were set to 3 min [see Fig. 1(b)]. After the 12 trials, two 3-min free-walking trials were conducted at slow and fast speeds.

C. Kinematic and Dynamic Models

In this section, we introduce kinematic and dynamic models that seek to describe the effects of knee joint misalignments on the wearer's gait pattern. These models will then be validated by the experimental results described in Section III. The models are restricted to the sagittal plane, i.e., the dominant plane of motion in human locomotion [22].

1) Revolute Knee Model: In the model illustrated in Fig. 2(a), hip and knee joints are regarded as simple revolute joints, human and robot hip joints are assumed aligned, and the shank orthosis is modeled as a slider and revolute joint. These assumptions are reasonable for ALEX II, since the shank cuff is smaller and more compliant than the thigh orthosis [see Fig. 1(a)], and, therefore, allows limited sliding on the soft tissues of the human shank and angular misalignments between the robotic and the human lower legs.

2) Elliptical Knee Model: In the tibiofemoral articulation, the point of contact on the tibial plateau slides posteriorly on the femoral condyles as the knee flexes [6]. Given the elongated shape of the posterior aspect of femur condyles, the human shank

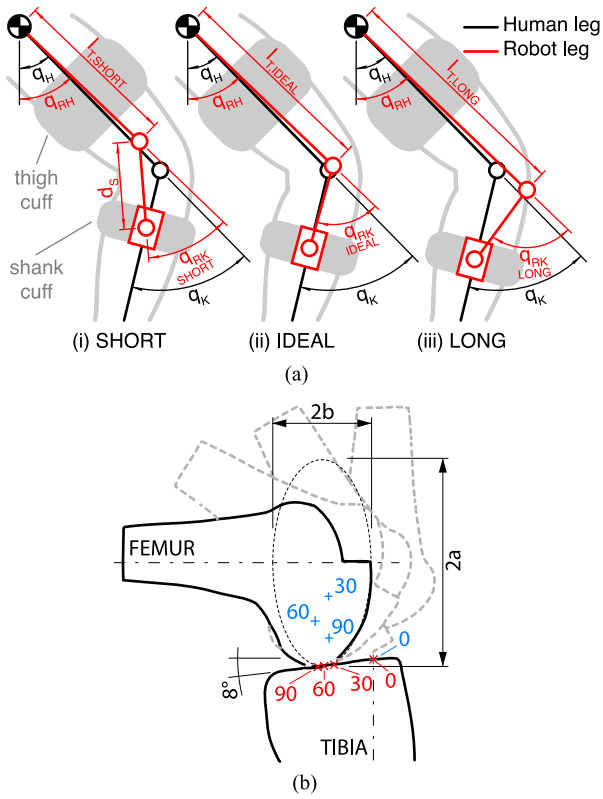

Fig. 2. (a) Relative position between the subject and the exoskeleton for *short*, *ideal*, and *long* alignments. Note that minimal misalignments are expected also in (ii) due to the compliance of the thigh interface (thigh cuff and human soft tissues). (b) Planar model of the human knee, adapted from [7]. a and b indicate the semimajor and semiminor axes of the ellipse used to approximate the femoral condyles. Red $\times$ indicates the estimated points of contact of the femur on the tibial plateau for some representative knee angles and blue $+$ shows the corresponding positions of the center of rotation of the femur relative to the tibia.

is actually moved away from the robot revolute joint as the knee flexes. The mismatch between the human tibiofemoral articulation and the robot revolute joint— which cannot be captured by the revolute knee model— should attenuate the effects caused by the robot thigh link being longer than the human thigh. To test for this hypothesis, we substituted the hinge joint representing the human knee in Fig. 2(a) with a more realistic planar joint [see Fig. 2(b)], by adapting the work of Yamaguchi and Zajac [7]. In their model, an elliptical arc describes the femoral condyles and a straight line, inclined 8° below the normal to the tibial longitudinal axis is used for the tibial plateau. These simple geometrical profiles are obtained by the interpolation of data measured on a male skeleton, and the point of contact of the femur along the tibial plateau is estimated by interpolating experimental data. In our implementation of the model, the eccentricity of the elliptical arc $e = \sqrt{1-(b/a)^2}$ and the ellipse scale factor are regarded as free parameters to be determined, subject by subject, through numerical optimization.

3) Dynamic Model: The ALEX II leg is modeled as a planar RR manipulator [23] whose equations of motion can be written as

$$\boldsymbol{\tau}_{\mathrm{m}} = M_{\mathrm{tot}}(\mathbf{q})\,\ddot{\mathbf{q}} + V(\mathbf{q},\dot{\mathbf{q}}) + G(\mathbf{q}) + F_{\mathrm{r}}(\mathbf{q},\dot{\mathbf{q}}) + \boldsymbol{\tau}_{\mathrm{Rint}} \quad (1)$$

[2]PASCO, Roseville, CA, USA.

$\mathbf{q} = [q_{\mathrm{RH}}, q_{\mathrm{RK}}]^T$ is the vector of the generalized coordinates of the robotic leg; q_{RH} yields the orientation of the thigh link with respect to a vertical axis pointing downward, and q_{RK} is the relative angle between the thigh and the shank links. Both angles are positive in the direction of anterior motion [see Fig. 2(a)]. $M_{\mathrm{tot}}(\mathbf{q}) \in \mathbb{R}^{2\times 2}$ is the overall mass matrix of the robotic leg (including the gear motors), $V(\mathbf{q}, \dot{\mathbf{q}}) \in \mathbb{R}^{2\times 1}$ contains Coriolis and centrifugal terms, $G(\mathbf{q})$, $F_{\mathrm{r}}(\mathbf{q}, \dot{\mathbf{q}}) \in \mathbb{R}^{2\times 1}$ are the vectors of gravity and friction torques, $\boldsymbol{\tau}_{\mathrm{Rint}} = [\tau_{\mathrm{RH}}, \tau_{\mathrm{RK}}]^T$ represents the human–robot interaction torques reflected at the joints of the robot, and $\boldsymbol{\tau}_{\mathrm{m}} \in \mathbb{R}^{2\times 1}$ is the vector of the driving torques, which can be thought of as the sum of the torques required to overcome actuators friction and inertia[3] and those required to move the robotic leg indicated as $\boldsymbol{\tau}$. To highlight these two contributions to $\boldsymbol{\tau}_{\mathrm{m}}$, (1) is rewritten as

$$\boldsymbol{\tau}_{\mathrm{m}} = M_{\mathrm{m}}\ddot{\mathbf{q}} + F_{\mathrm{r}}(\mathbf{q}, \dot{\mathbf{q}}) + \boldsymbol{\tau} \tag{2a}$$

$$\boldsymbol{\tau} = \boldsymbol{\tau}_I + G(\mathbf{q}) + \boldsymbol{\tau}_{\mathrm{Rint}} \tag{2b}$$

where $M_{\mathrm{m}}(\mathbf{q}) \in \mathbb{R}^{2\times 2}$ is the mass matrix of the gear motors and $\boldsymbol{\tau}_I \in \mathbb{R}^{2\times 1}$ includes the inertial torques arising from the motion of the robotic leg

$$\boldsymbol{\tau}_I = M_{\mathrm{r}}(\mathbf{q})\,\ddot{\mathbf{q}} + V(\mathbf{q}, \dot{\mathbf{q}}) \tag{3}$$

and $M_{\mathrm{r}}(\mathbf{q}) \in \mathbb{R}^{2\times 2}$ is the mass matrix of the robotic leg (not including the motors).

$\boldsymbol{\tau}_{\mathrm{Rint}}$ consists of τ_{RH} and τ_{RK}, the interaction torques reflected at the robot hip and knee joints. These can be computed from the force/torques measured at the leg orthoses, i.e., the interfaces with the user

$$\tau_{\mathrm{RH}} = -d_{\mathrm{T}} F_{x,\mathrm{T}} - M_{z,\mathrm{T}} + \tau_{\mathrm{RK}} - l_T F_{x\mathrm{T,S}} \tag{4a}$$

$$\tau_{\mathrm{RK}} = -d_{\mathrm{S}} F_{x,\mathrm{S}} - M_{z,\mathrm{S}}. \tag{4b}$$

In the previous equations, we adopted a human-centered convention for assigning the sign of τ_{RH} and τ_{RK}; a positive hip interaction torque indicates a torque exerted by the robot on the human hip, which tends to flex the hip. A positive knee interaction torque indicates a torque exerted by the robot on the human knee, which tends to extend the knee. $\mathbf{W}_* = [F_{x,*},\ F_{y,*},\ M_{z,*}]^T \in \mathbb{R}^{3\times 1}$ are force/torques measured by the thigh (subscript T) or shank (subscript S) sensors: $F_{x,*}$ being orthogonal to the robotic link and directed anteriorly, $F_{y,*}$ being parallel to the robotic link and directed proximally, and $M_{z,*}$ acting on the *xy* (sagittal) plane. d_* is the moment arm of $F_{x,*}$ and $F_{x\mathrm{T},S}$ is the projection of the interaction force at the shank (F_{S}) onto the thigh *x*-axis:

$$F_{x\mathrm{T,S}} = \cos q_{\mathrm{RK}}\, F_{x,\mathrm{S}} - \sin q_{\mathrm{RK}}\, F_{y,\mathrm{S}}. \tag{5}$$

Fig. 3 illustrates a schematic of the lower level controller of ALEX II. When the device operates in transparent mode (i.e., $\boldsymbol{\tau}_{\mathrm{des}} = \mathbf{0}$) and only the inner feedback loop is active, the controller seeks to drive the error $(G(\mathbf{q}) - \boldsymbol{\tau})$ to zero (i.e., the torques at the output shafts of the gear motors match the gravity torques). $G(\mathbf{q})$ is estimated by a gravity model, and $\boldsymbol{\tau}$ is measured by single-axis torque sensors mounted on the output shaft

[3]We assume friction to be mostly due to the gearboxes and negligible elsewhere.

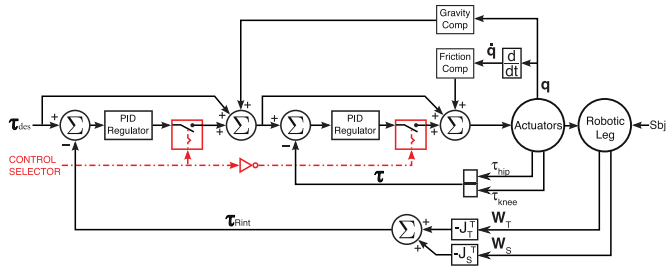

Fig. 3. Controllers used to simulate the UI (inner feedback loop) and CI (outer feedback loop) conditions [14]. Note that these controllers share friction and gravity compensation terms. A software selector allows us to alternatively activate the two control strategies.

of each gear motor. Assuming that all disturbances are inside the closed-loop rejection bandwidth of the controller and that the gravity model is accurate, (2b) indicates that the user is in charge of providing $\boldsymbol{\tau}_I$, the inertial torques needed to accelerate or decelerate the robotic leg. We refer to this control mode as *UI*. Conversely, when only the outer feedback loop is active, the controller seeks to drive the interaction error $(\boldsymbol{\tau}_{\mathrm{des}} - \boldsymbol{\tau}_{\mathrm{Rint}})$ to zero—as estimated from (4) and the readings of the force/torque sensors—thereby masking inertial torques to the user (*compensated robot inertia* or *CI*). In practice, due to the limitation of the controller, only a partial cancellation is obtained (on average, a reduction of about 52% at the hip joint, and about 46% at the knee joint; see Section III-A).

D. Data Analysis

Data from position and force/torque sensors were collected at 1 kHz and low-pass filtered online with a first-order Butterworth filter (goniometers: $f_c = 10$ Hz, force/torque transducers: $f_c = 12$ Hz). Only the last 60 s of each session was considered for postprocessing. Gait segmentation was performed through foot switches, the kinematic models were validated by comparing measured angular data with corresponding estimates from the models, and a set of metrics was computed to address average changes in interaction forces, human and robot kinematics, and gait timing across the trials. Data collected during the free-walking sessions are not included in this paper.

We analyzed the average magnitudes of the interaction forces/torques at the shank ($|F|_{\mathrm{S}}$, $|M|_{\mathrm{S}}$) and thigh ($|F|_{\mathrm{T}}$, $|M|_{\mathrm{T}}$) orthoses, together with the root mean square (RMS) of the interaction torques reflected at the powered joints (τ_{RH}, τ_{RK}). As suggested by (4), the latter variables capture only the components of the interaction forces/moments that directly contribute to the motion of the robotic leg, whereas the former account for *all* the interaction components, including those that do not generate torque at the powered joints, and yet may be important for the wearer's safety and comfort. Since the robot was operated in transparent mode, any (undesired) nonzero interaction was assumed to be due to the three independent variables, neglecting any unmodeled effects (e.g., nonideal behavior of the controller).

Optical encoders and potentiometric goniometers were used to measure the robot and the human sagittal joint angles, respectively. For each subject, position data were time normalized

TABLE I
RESULTS OF THE STATISTICAL ANALYSIS (NS= NONSIGNIFICANT, IN= INERTIA, SP= SPEED, A= ALIGNMENT, S= SHORT, I= IDEAL, L = LONG, CI = COMPENSATED INERTIA)

	Three-way repeated measures ANOVA p-value							Pairwise comparison t(8)			*In* = CI, *Sp* = slow, *A* = ideal
	In	**Sp**	**A**	**In*Sp**	**In*A**	**Sp*A**	**In*Sp*A**	**I-S**	**I-L**	**S-L**	**(Mean ± SD)**
$\lvert F\rvert_T$	**<0.05**	**<0.0001**	**<0.01**	**<0.01**	ns	ns	ns	**−3.25**	0.738	**3.819**	43.2 ± 10.6 N
$\lvert M\rvert_T$	**<0.01**	**<0.001**	**<0.01**	**<0.01**	ns	ns	ns	**−4.382**	0.489	**4.212**	5.3 ± 0.9 N·m
τ_{RH}	**<0.00001**	**<0.001**	ns	**<0.001**	ns	ns	**<0.05**	–	–	–	6.9 ± 1.4 N·m
$\lvert F\rvert_S$	**<0.01**	**<0.05**	ns	ns	ns	ns	ns	–	–	–	40.3 ± 12.1 N
$\lvert M\rvert_S$	**<0.0001**	**<0.001**	ns	ns	ns	ns	ns	–	–	–	2.5 ± 0.7 N·m
τ_{RK}	**<0.0001**	**<0.0001**	ns	ns	ns	ns	ns	–	–	–	3.1 ± 0.7 N·m
ROM_H	ns	**<0.01**	ns	ns	ns	ns	ns	–	–	–	45.7° ± 10.2°
ROM_{RH}	**<0.01**	**<0.00001**	ns	**<0.05**	ns	ns	ns	–	–	–	40.9° ± 5.4°
JRR_H	**<0.01**	ns	ns	ns	ns	**<0.05**	ns	–	–	–	1.11 ± 0.14
ROM_K	**<0.05**	ns	ns	ns	ns	**<0.05**	ns	–	–	–	78.6° ± 11.4°
ROM_{RK}	**<0.05**	**<0.05**	**<0.05**	ns	**<0.05**	ns	ns	**2.532**	**−3.716**	**−3.191**	78.9° ± 5.9°
JRR_K	ns	**<0.001**	**<0.05**	ns	ns	ns	ns	−2.181	1.631	**3.124**	1.00 ± 0.11
T_{str}	**<0.001**	**<0.00001**	ns	**<0.05**	ns	ns	ns	–	–	–	1.37 ± 0.11 s
$STSW_r$	**<0.0001**	**<0.05**	ns	ns	ns	ns	ns	–	–	–	0.97 ± 0.12

over the gait cycle (0%–100% GC) and averaged to obtain joints angular trajectories. These trajecotries were then fed into the revolute knee model, and the estimated trajectory of the robot knee joint (i.e., the output of the model) was compared with the corresponding measured average trajectory. The inputs to the elliptical knee model were the same as those of the revolute knee model; however, the RMS values of the kinematic error (i.e., the mismatch between measured and estimated robot knee angles) at each alignment were summed together to yield an overall cost function, and an unconstrained optimization was conducted using MATLAB[4] to obtain the optimal eccentricity and scale factor of the approximated condylar profiles [see Fig. 2(b)].

The ranges of motion of the human hip and knee (ROM_H, ROM_K) and those of the robotic leg (ROM_{RH}, ROM_{RK}) over the gait cycle were computed, along with the ratios between the human and robotic joint ranges (JRR_H, JRR_K). These ratios were selected since they are sensitive to small differences between human and robotic ROM.

As measures of gait timing and temporal symmetry, the stride period (T_{str}) and the ratio of the stance-to-swing ($STSW_r$, left leg over right leg) were analyzed [15], [24].

All scalar variables yielded a single value per stride. Values corresponding to the strides occurring in the last 60 s of each session were averaged to obtain a single value per session per each subject. Nondimensionless variables were normalized to a common *reference trial* (*In* = CI, *Sp* = slow, *A* = ideal) prior to the computation of the group averages, and a three-way repeated-measures ANOVA was employed to identify any significant effects ($\alpha = 0.05$) of the factors *In*, *Sp*, and *A* on the metrics described previously, and potential interactions among the three factors. Post hoc comparisons with Bonferroni–Holm correction were carried out where appropriate. All the statistical tests were conducted using SPSS.[5]

[4]The MathWorks, Natick, MA, USA, USA.
[5]IBM Corp., Armonk, NY, USA.

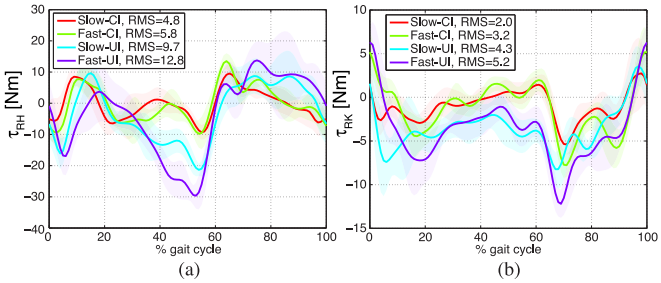

Fig. 4. Group averages of the interaction torques reflected at the (a) hip and (b) knee robot joints. Data from different alignments have been merged, shaded areas indicate ±1 SD. RMS values of each torque profile are reported in the legends.

III. RESULTS

Results of the ANOVA are illustrated in Table I, along with the *t*-statistics from post hoc comparisons calculated from the marginal means. Significant results are marked in bold font. Group averages of all the metrics for the reference trial are also reported in Table I.

A. Robot–Human Interaction forces

Robot inertia significantly increased all interaction forces and torques ($\lvert F\rvert_S$, $\lvert M\rvert_S$, $\lvert F\rvert_T$, $\lvert M\rvert_T$), as well as the equivalent torques reflected at the powered joints (τ_{RH} and τ_{RK}), as confirmed by significant main effects of inertia in these variables. When inertia is not actively compensated, the user must generate the torques required to accelerate or decelerate the robotic leg (3); thereby, the increase in the magnitude of robot–human interactions evidenced by experimental results in Figs. 4 and 5(a)–(d). The group averages of τ_{RH} and τ_{RK} shown in Fig. 4 support previous findings presented in [14].

Walking speed significantly affected all interaction metrics. Faster speed resulted in increased cadence and step length (see Sections III-B and III-C), and, thereby, larger inertial torques arisen from the robotic leg, which were counteracted by interaction torques of opposite sign in UI mode.

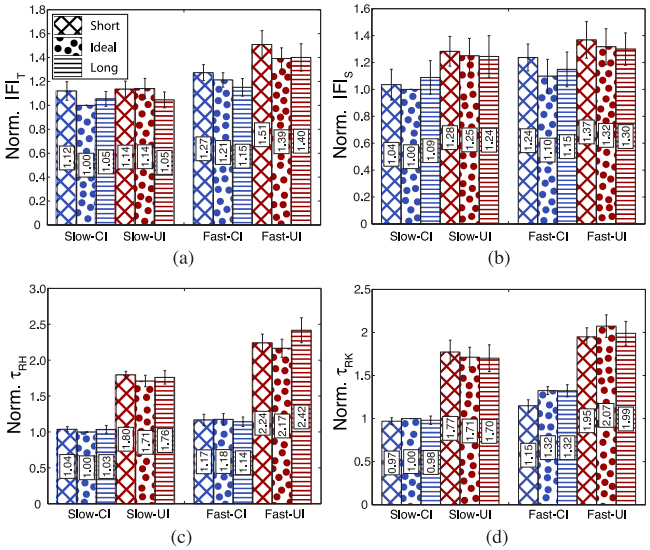

Fig. 5. Average magnitudes of the interaction forces at the thigh (a) and shank (b) orthoses, and torque reflected at the (c) hip and (d) knee joints. Error bars indicate ± 1 SE.

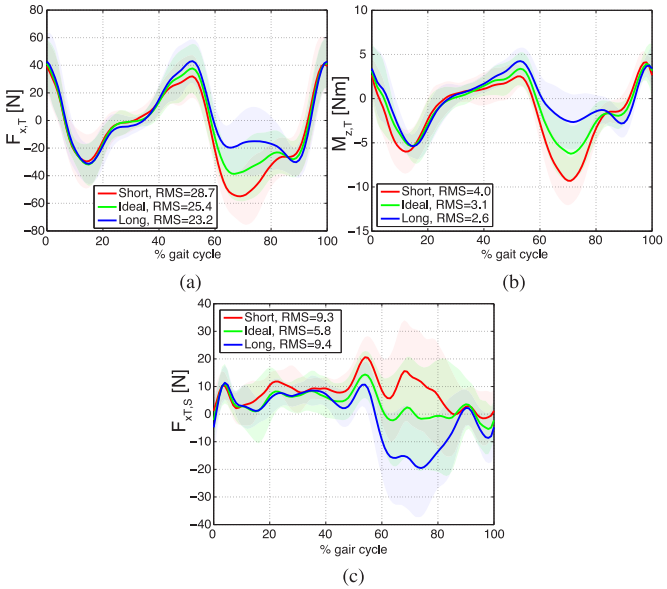

Fig. 6. Group averages of (a) $F_{x,\mathrm{T}}$, (b) $M_{z,\mathrm{T}}$, and (c) $F_{x\mathrm{T,S}}$ for different alignments. Shaded areas indicate ± 1 SD, RMS values of each force profile are reported in the legends.

Interestingly, alignment of the knee joint significantly affected interaction forces and torques at the thigh [see Fig. 5(a)], but not those at the shank— possibly due to the higher compliance of the shank orthosis compared with the thigh orthosis. Post hoc comparisons evidenced larger $|F|_{\mathrm{T}}$ and $|M|_{\mathrm{T}}$ for the *short* alignment compared with the other two.

CI mode partially masked robot inertia to the user; thus, substantially reducing the relative increments in the interaction metrics due to walking speed [see Fig. 5(a) and (c)]. This was evidenced by the significant interaction (*In*Sp*) found in all the thigh metrics. As for the shank and knee metrics, the effect of speed was not influenced by inertia compensation. The dynamic model (3) applied to experimental data (i.e., the measured $\mathbf{q}, \dot{\mathbf{q}}, \ddot{\mathbf{q}}$) showed that the impact of walking speed on $\boldsymbol{\tau}_I$ was indeed much more prominent at the hip joint (average increase in the RMS torque: 2.53 N) than it was at the knee joint (average increase: 0.38 N·m). This was mainly due to the moment of inertia of the shank link about the knee axis being much smaller than the overall moment of inertia of the robotic leg about the hip axis ($15.7 \leqslant M_{\mathrm{r}}(1,1)/M_{\mathrm{r}}(2,2) \leqslant 22.6$ for ALEX II depending on the knee angle). Even when robot inertia was not compensated, the *additional* knee interaction torque experienced by users when they walked at faster speed was relatively small (i.e., within intrasubject variability), thereby the lack of significant interaction *In*Sp* [see Fig. 5(d)].

There was a significant third-order interaction *In*Sp*A* in the torque reflected at the hip joint τ_{RH} [see Fig. 5(c)]. Two separate two-way ANOVA (UI mode and CI mode) evidenced that the impact of alignment on τ_{RH} was significant in UI mode ($p < 0.05$) but not in CI mode. Specifically, post hoc comparisons confirmed that τ_{RH} was significantly smaller in the *ideal* alignment compared with the *long* one when inertia compensation was disabled. Indeed, an increase in the length of the robot thigh l_{T} produces a corresponding increase in the moment of inertia of the thigh link about the hip joint, thus amplifying the hip inertial torques described by (3). The moment of inertia of the robotic leg about the hip flexion/extension axis varied with the knee angle within each gait cycle (intrasubject variability) and with the adjustments of the robotic links (intersubject variability). Taking into account both sources of variability, the average moment of inertia of the robotic leg about the hip flexion/extension axis was estimated as $1.28 \pm 0.11\ \mathrm{kg \cdot m^2}$ in the *ideal* alignment; the *short* alignment reduced this value by $8 \pm 1\%$, while the *long* alignment caused an average increase of $9\% \pm 1\%$. In UI mode, inertial torques are counteracted by equal and opposite torques generated entirely by the wearer (see Section II-C), these produced larger τ_{RH}. Conversely, any variation in the mass matrix M_{r} due to an adjustment of the thigh length l_{T} impacted τ_{RH} to a lesser extent when robot inertia was partly compensated, thereby the lack of main effect of alignment in CI mode.

Overall, the results described previously show that: 1) regardless of whether the robot inertia was compensated or not, increasing the length of the robot thigh from *short* to *ideal* or *long* reduced the magnitude of the interaction forces and moments at the thigh orthosis $|F|_{\mathrm{T}}$ and $|M|_{\mathrm{T}}$; 2) in UI mode, τ_{RH} increased in the *long* alignment, but it was not affected in the CI mode; 3) $|F|_{\mathrm{S}}$, $|M|_{\mathrm{S}}$, τ_{RK} did not depend on the alignment. Decreases in $|F|_{\mathrm{T}}$ and $|M|_{\mathrm{T}}$ were mainly due to $F_{x,\mathrm{T}}$ and $M_{z,\mathrm{T}}$ and were localized in midswing, when the swing-phase peak knee flexion takes place (see Fig. 6). In midswing, the torques τ_{RH} and τ_{RK} due to robot inertia tended to flex the human hip and knee joints (see Fig. 4). These torques were counteracted by the user's reactions at the thigh (posteriorly directed forces $F_{x,\mathrm{T}} < 0$, $M_{z,\mathrm{T}} < 0$) and shank (anteriorly directed forces $F_{x,\mathrm{S}} > 0$, $M_{z,\mathrm{S}} > 0$) as described by (4). The first two terms in (4a) were, therefore, positive in midswing, while the third one τ_{RK} was negative. τ_{RK} did not change significantly with alignment, nor did $|F_{\mathrm{S}}|$. However, as l_{T} increased, an amplified peak flexion angle q_{RK} (see Section III-B) caused the projection $F_{x\mathrm{T,S}}$ to change sign from positive (i.e., acting against the thigh reactions) to negative (i.e., acting in the same direction as the thigh reactions)

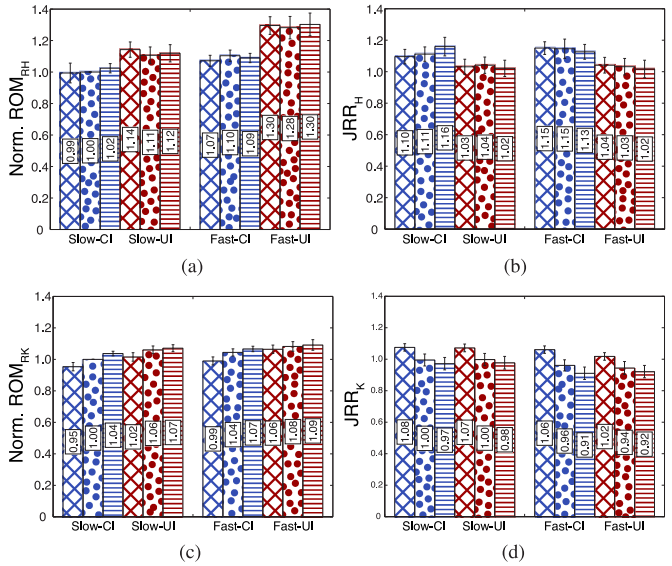

Fig. 7. (a) ROM of the robotic hip, (b) ratio of human and robotic hip ROM $\mathrm{JRR_H}$, (c) ROM of the robotic knee, and (d) ratio of human and robotic knee ROM $\mathrm{JRR_K}$. Error bars indicate ± 1 SE.

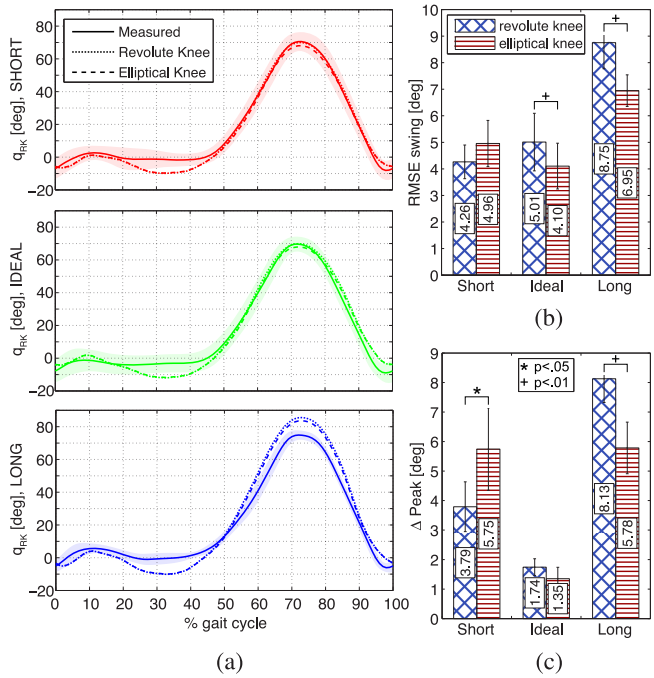

Fig. 8. (a) Measured and estimated profiles of the robot knee angle for sbj. 2 in the short, ideal, and long alignments (shaded areas indicate ± 1 SD). (b) Group averages of the estimation errors for the peak flexion angle of the robot knee. (c) Group averages of the estimation errors for the flexion angle of the robot knee during swing. Note that, unlike in (1)–(5), here we adopt the biomechanics convention by which a positive knee angle indicates flexion [15].

[see Fig. 6(c)]. The effect of $F_{x\mathrm{T,S}}$ on τ_{RH} was further amplified by a longer l_{T}. For these two reasons, the user was capable of driving the robotic leg with significantly smaller $|F|_{\mathrm{T}}$ and $|M|_{\mathrm{T}}$, even though the required τ_{RH} stayed approximately the same (*CI* mode) or increased (*UI* mode) with a long l_{T}.

B. Gait Kinematics

Both $\mathrm{ROM_H}$ and $\mathrm{ROM_{RH}}$ significantly increased with the speed [see Fig. 7(a)], confirming the known positive correlation between walking speed and hip range of motion [15], [25].

Robot inertia significantly affected $\mathrm{JRR_H}$ [see Fig. 7(b)]; when inertia compensation was disabled, the ratio was smaller, mainly due to a significant increase in $\mathrm{ROM_{RH}}$, while $\mathrm{ROM_H}$ increased only slightly. Prior to push off, the fully extended human leg had to decelerate the robot first, and, then, accelerate it in the opposite direction to get ready for the swing phase. The initiation of hip flexion, then, occurred at larger hip extension angles, producing the observed increase in $\mathrm{ROM_{RH}}$. The effects of inertia were amplified at fast walking speed, especially if inertia compensation was disabled; thereby, the synergistic effects of speed and inertia on $\mathrm{ROM_{RH}}$ evidenced by the significant interaction *In*Sp*.

There was a crossover interaction *Sp*A* on $\mathrm{JRR_H}$, due to a positive correlation between this ratio and the length of the thigh link l_{T} at moderate speed, which turned into a negative correlation at fast speed. Separate two-way repeated-measures ANOVA, however, found no significant effects of alignment at either speeds.

As for the knee joint, robot inertia significantly increased $\mathrm{ROM_K}$ and $\mathrm{ROM_{RK}}$ [see Fig. 7(c)] by a similar factor— as indicated by $\mathrm{JRR_K}$ not depending on robot inertia [see Fig. 7(d)]. During midswing, when the peak knee flexion takes place, inertia of the robotic leg helps flexion of the hip, and resists the action of the knee extensors that decelerate the flexing lower leg [14]. This produces larger peak flexion angles, and, in turn, increased $\mathrm{ROM_K}$ and $\mathrm{ROM_{RK}}$.

Walking speed significantly increased $\mathrm{ROM_{RK}}$, but had no significant effects on $\mathrm{ROM_K}$ as also confirmed by a decreasing $\mathrm{JRR_K}$. As walking speed increases, the swing-phase peak knee flexion angle increases far less than the stance-phase peak flexion angle [15], [26]. Since the latter has no effect on the ROM, this may explain the lack of significant increase in human knee ROM due to speed.

$\mathrm{JRR_K}$ was close to unity at ideal alignment, indicating a good matching of robot and human knee trajectories. A main effect of alignment was found in $\mathrm{ROM_{RK}}$— the thigh link, the larger the ROM of the robotic knee [see Fig. 7(c)]. This was also confirmed by $\mathrm{JRR_K}$ whose values significantly decreased from *short* to *long* alignments [see Fig. 7(d)]. Increase in $\mathrm{ROM_{RK}}$ corresponded to progressively larger peak knee flexion angles as the length of the robot link changed from *short* to *long*. As l_{T} increases (while d_{T} is constant), the shank cuff is attached more and more distally along the lower leg for any given position of the robot thigh relative to the human thigh [see Fig. 2(a)]. This produces larger flexion angles of the robot knee. Fig. 8(a) shows the average robot knee angles measured in a representative subject for each alignment (solid lines), along with the output of the revolute knee model (dotted line). It may be noticed that this simple model captures quite well the increasing trend in the peak flexion angle shown by the measured data, nonetheless it overestimates the peak flexion angle in the *long* alignment.

The mismatch between human articulation and the robot revolute joint—which cannot be captured by the revolute knee model—attenuates the effects of a long l_{T} on $\mathrm{ROM_{RK}}$. Indeed,

Fig. 7(d) shows that JRR_K values in the *long* alignment are consistently closer to the *ideal* ones than these corresponding to the *short* alignment. Post hoc comparisons confirmed significant differences between the *short* and *long* alignments in the same metric, while no significant differences were found between *ideal* and *long* alignments. To further support the previous assertion, the outputs of the elliptical knee model are presented in Fig. 8(a), where the same experimental data fed into the revolute knee model were used as inputs. Wilcoxon signed-rank tests were performed to compare the performances of the revolute knee model to these of the elliptical knee model. Compared with the former, the latter model significantly reduced the swing-phase RMS error in the knee angle, both in the ideal and in the long alignment, while the two models performed similarly in the short alignment [see Fig. 8(b)]. In terms of peak knee flexion angle, the elliptical knee model outperformed the revolute knee model in the long alignment, but was significantly less accurate in the short alignment [see Fig. 8(c)]. In terms of RMS error over the full gait cycle, results resembled the ones on the peak knee flexion angle, with the revolute knee model performing significantly better than the elliptical knee model in the short alignment ($6.10^\circ \pm 2.16^\circ$ versus $6.62^\circ \pm 2.40^\circ$), slightly better in the ideal alignment, and significantly worse in the long alignment ($7.56^\circ \pm 1.21^\circ$ versus $6.78^\circ \pm 1.05^\circ$).

Overall, the previous analysis reveals that inertia of the robotic leg and alignment of the knee joint have a similar effect on the kinematics of the robot knee joint, namely they both increase the swing-phase peak flexion angle, thereby augmenting ROM_{RK} [see Fig. 7(c)]. In the first case, inertial torques arise that resist deceleration of the lower leg at midswing, thereby delaying initiation of knee extension. In the second case, a longer thigh link results in increased ROM_{RK} for any given orientation of the human knee, for a purely kinematic reason. However, as discussed in Section III-A, changing l_T affects the mass distribution of the robot leg; thereby, creating a coupling between the two factors, inertia and alignment, as evidenced by a significant interaction (*In*A*). Separate two-way repeated-measures ANOVA showed significant effects of alignment for both *UI* mode ($p < 0.05$) and *CI* mode ($p = 0.05$) further supporting this observation.

A significant interaction (*Sp*A*) was detected in ROM_K. Subsequent two-way repeated-measures ANOVA conducted on moderate and fast speed separately revealed no significant effects of the factor alignment, therefore these data were not analyzed further.

C. Gait Timing

Stride time decreased from slow to fast speed [see Fig. 9(a)], confirming a well-known trend of human walking [15]. Additionally, T_{str} increased significantly with robot inertia. Inertial contributes are augmented by speed, but these contributes actually contrast the main effects of walking speed on T_{str}, namely, they tend to increase T_{str}. This was evidenced by a significant *In*Sp* interaction, indicating that the effect of speed was amplified when inertia was partially masked to the wearer (see Table I).

Temporal symmetry was negatively impacted by the inertia of the robotic leg (which acted on the left leg only) and by speed,

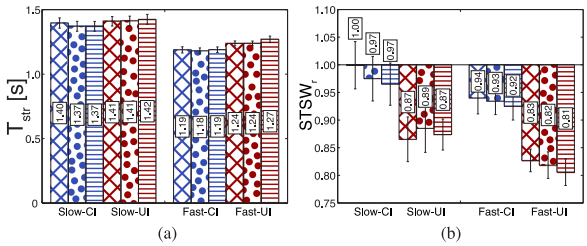

Fig. 9. (a) Stride period and (b) temporal gait symmetry as expressed by the stance-to-swing ratio (left leg/right leg).

the lack of significant interactions suggesting that the effects of the two factors were approximately additive [see Fig. 9(b)]. Increases in stride and swing periods as a consequence of augmenting the natural moment of inertia of the human leg have been reported in previous studies, using weights [27], [28], or a passive mechanism [29], or powered exoskeletons [13], [14]. With a longer swing time on the left leg, the corresponding STSW decreased; thus, reducing the overall STSW ratio as evidenced in this study. This, in turn, indicated that subjects's weight was mostly supported by the right leg [14], [17], [30], [31].

No significant effects of alignment were observed for the timing metrics, suggesting that gait timing is robust to small misalignments between the user and the robot.

IV. Discussion

The effects of human–robot misalignment have rarely been explored in the literature. The rationale behind studies on this topic encompasses mitigation of wearer's discomfort and potential safety hazards, and reduction of the time required to fit the wearer into the exoskeleton.

Previous works focused on the upper extremities, and developed design approaches that resulted in self-aligning passive auxiliary linkages. A common drawback of these linkages is that they all increase design complexity and mechanical impedance compared with traditional exoskeletons. Increased mass, in particular, is critical for machines interacting with human users, since it amplifies the risk of injuries in case of failure [32]. It is, therefore, important to find the best tradeoff between a theoretically *misalignment free*, but bulky and complex architecture on one side, and a simpler traditional design with limited mechanical complexity, friction, and inertia on the other side. To pursue this goal, a deeper understanding of the effects of misalignment on the user must be achieved on an application-by-application basis. Unlike previous research, we focused on the lower extremities (more precisely, on the knee articulation), and adopted a model-driven human-oriented perspective. Motivated by the idea that a better understanding of the effects of human–robot misalignment can drive the design of future improved exoskeletons, this study analyzed the effects of knee misalignments on a user's gait in terms of kinematics, kinetics, and gait timing.

To date, most treadmill-based rehabilitation exoskeletons feature a simple hinge joint at the robotic knee: Lokomat [1], LOPES [33], ALEX I, II, and III [18], [34], [35], and AutoAmbulator [36]. Each device provides several adjustments to fit the subject's legs into the robot and reduce macromisalignments. The user is connected to the robot via a semirigid thigh

cuff and single (ALEX II, ALEX III, AutoAmbulator) or double (Lokomat, LOPES) shank cuffs or shoe inserts (ALEX I) whose deformations can accommodate small misalignments.

While a proper self-aligning knee mechanism can be added to these designs by, e.g., implementing auxiliary DOF on the shank orthosis as illustrated in Fig. 2(a), experimental results presented in this paper suggest that the traditional approach may be sufficient to guarantee the wearer's comfort, even in the presence of significant knee misalignments, namely the effects of misalignment may be attenuated by the compliance of the cuffs, which augments the compliance of the human soft tissues.

Proper self-aligning mechanisms may reduce misalignments at the expenses of increased robot inertia. For instance, a lumped mass $m = 1$ kg added at the knee of ALEX II would increase the moment of inertia of the leg about the hip flexion–extension axis by approximately 20%. *Results presented in this study tend to discourage the use of such approaches in lower limb exoskeletons, unless the additional inertia is masked to the wearer by control*—a strategy that requires the use of expensive force/torque sensors. Indeed, in terms of statistical significance, the effects of robot inertia on the user's gait were much more marked than those of misalignment, despite the latter being purposely exaggerated compared with what can be reasonably expected during a rehabilitative session. Robot inertia significantly increased undesired interaction forces/torques at the thigh and shank orthoses, the ranges of motion of the robotic hip joint, and those of the robotic and human knee joints. These effects were further amplified by fast walking speed. Robot inertia also altered the natural increase in cadence that occurs at faster walking speed and disrupted temporal symmetry of gait.

Interestingly, the gait pattern of young healthy subjects appeared to be "robust" to knee misalignments; significant changes were not found in human gait timing or kinematics. A robot thigh longer than the human one increased the range of motion of the robotic knee due to kinematic coupling—the effect being amplified by the inertia of the robotic leg—however, alignment did not affect the range of motion of the human knee. *The most relevant effects of knee misalignments consisted of changes in the interaction forces and torques at the thigh orthosis.* A longer robot thigh was found to increase the equivalent interaction torque at the hip joint compared with the aligned case, but this only happened when robot inertia was not compensated, suggesting that this effect was due to the increased inertia of the longer robot thigh, rather than by the knee misalignment itself. Compared with the short alignment, the long alignment resulted in a significant reduction of the undesired interaction forces and moments measured at the thigh cuff, which was achieved without a corresponding increment of the interaction forces at the shank, due to a larger mechanical advantage of the latter to the torque reflected at the hip joint. Moreover, the mismatch caused by a longer robotic leg was partially compensated by the human knee articulation, wherein the elongated shape of the posterior aspect of femur condyles increases the equivalent length of the human thigh as the knee flexes. *Therefore, this analysis suggests that: 1) the effects of human–robot knee misalignments on the wearer's gait can be minimized if inertia compensation is implemented, and 2) an excessively long robot thigh is preferable to an excessively short one.*

This study aimed to identify the effects of robot–human knee misalignment on a user's gait, and how these would change with robot inertia and walking speed. We, therefore, prioritized the goal of testing three factors (and their combinations) over short walking bouts rather than testing fewer factors over prolonged training sessions. Even though healthy subjects usually adapt to additional leg inertia in approximately 50 strides [28], walking in an exoskeleton controlled in *transparent mode* might require a longer adaptation period. This might have prevented us from fully assessing subjects' motor adaptation to the (misaligned) robotic leg. Similarly, discomfort caused by misalignment—which was not reported by any of the subjects—might instead occur over longer training sessions. In this study, the device was set to *transparent mode*—a control strategy common to all exoskeletons that feature the force control. This choice allowed us to reach few conclusions that can be considered valid for most lower limb powered exoskeletons. However, the effects of knee misalignments occurring when the robot operates in *assistive mode* cannot be directly inferred from the results presented here, and further experimental work will be required to address this point. Future research will also seek to determine how knee joint misalignments directed along the longitudinal axis of the femur (as the ones targeted by this study) compared with those orthogonal to the same axis.

V. Conclusion

To the best of the authors' knowledge, this study is the first one specifically addressing the effects of human–robot misalignment on the gait of healthy subjects. We introduced controlled misalignments at the knee joint of a treadmill-based exoskeleton, and measured the changes on the kinematics, kinetics, and timing of the users' gait, explaining these changes with the help of simple kinematic and dynamic models. The experimental design adopted in this study allowed us to quantify correlations between misalignment, robot inertia, and walking speed.

Recent trends in the design of upper limb exoskeletons rely on the introduction of passive auxiliary mechanisms to attenuate misalignments at the shoulder and elbow joints. We showed that such mechanisms might not be required in the case of exoskeletons for the lower limbs, provided that semirigid orthoses are utilized to connect the human legs to the robot, and the robot inertia is actively compensated. Significant effects of knee misalignment were found especially on the interaction forces at the thigh interface, and these were amplified by robot inertia. As far as the knee articulation is concerned, our analysis pointed out that a robot thigh, which is longer than the nominal length, is less critical than a shorter one for subject's comfort.

References

[1] G. Colombo, M. Joerg, R. Schreier, and V. Dietz, "Treadmill training of paraplegic patients using a robotic orthosis," *J. Rehabil. Res. Dev.*, vol. 37, no. 6, pp. 693–700, 2000.

[2] K. Kong and D. Jeon, "Design and control of an exoskeleton for the elderly and patients,"*IEEE/ASME Trans. Mechatronics*, vol. 11, no. 4, pp. 428–432, Aug. 2006.

[3] H. Kazerooni and R. Steger, "The berkeley lower extremity exoskeleton," *J. Dyn. Syst., Meas., Control*, vol. 128, no. 1, pp. 14–25, 2006.

[4] J. Morrison, "The mechanics of the knee joint in relation to normal walking," *J. Biomech.*, vol. 3, no. 1, pp. 51–61, 1970.

[5] C. Wheeless, *Wheeless' Textbook of Orthopaedics*. Brooklandville, MD, USA: Data Trace Publishing Company, 1996.
[6] G. L. Smidt, "Biomechanical analysis of knee flexion and extension," *J. Biomech.*, vol. 6, no. 1, pp. 79–92, 1973.
[7] G. T. Yamaguchi and F. E. Zajac, "A planar model of the knee joint to characterize the knee extensor mechanism," *J. Biomech.*, vol. 22, no. 1, pp. 1–10, 1989.
[8] M. A. Bridge, W. D. Stanish, D. R. Russell, and J. Morash, "Knee bracing in sports medicine: A review," *Techn. Knee Surg.*, vol. 7, no. 4, pp. 251–260, Dec. 2008.
[9] N. Jarrassé and G. Morel, "Connecting a human limb to an exoskeleton," *IEEE Trans. Robot.*, vol. 28, no. 3, pp. 697–709, Jun. 2012.
[10] A. Schiele and F. C. van der Helm, "Kinematic design to improve ergonomics in human machine interaction," *IEEE Trans. Neural Syst. Rehabil. Eng.*, vol. 14, no. 4, pp. 456–469, Dec. 2006.
[11] A. H. Stienen, E. E. Hekman, F. C. Van Der Helm, and H. Van Der Kooij, "Self-aligning exoskeleton axes through decoupling of joint rotations and translations," *IEEE Trans. Robot.*, vol. 25, no. 3, pp. 628–633, Jun. 2009.
[12] M. Cempini, S. M. M. De Rossi, T. Lenzi, N. Vitiello, and M. C. Carrozza, "Self-alignment mechanisms for assistive wearable robots: A kinetostatic compatibility method," *IEEE Trans. Robot.*, vol. 29, no. 1, pp. 236–250, Feb. 2013.
[13] G. Aguirre-Ollinger, J. Colgate, M. Peshkin, and A. Goswami, "Design of an active one-degree-of-freedom lower-limb exoskeleton with inertia compensation," *Int. J. Robot. Res.*, vol. 30, no. 4, pp. 486–499, 2011.
[14] D. Zanotto, T. Lenzi, P. Stegall, and S. Agrawal, "Improving transparency of powered exoskeletons using force/torque sensors on the supporting cuffs," presented at the IEEE Int. Conf. Rehabilitation Robotics, Seattle, WA, USA, Jun. 24–26, 2013.
[15] D. A. Winter, *The Biomechanics and Motor Control of Human Gait: Normal, Elderly and Pathological*. Waterloo, ON, USA: Waterloo Univ. Press, 1991.
[16] K. N. Winfree, P. Stegall, and S. K. Agrawal, "Design of a minimally constraining, passively supported gait training exoskeleton: ALEX II," in *Proc. IEEE Int. Conf. Rehabil. Robot.*, 2011, pp. 1–6.
[17] D. Zanotto, G. Rosati, S. Spagnol, P. Stegall, and S. Agrawal, "Effects of complementary auditory feedback in robot-assisted lower extremity motor adaptation," *IEEE Trans. Neural Syst. Rehabil. Eng.*, vol. 21, no. 5, pp. 775–786, Sep. 2013.
[18] P. Stegall, K. Winfree, D. Zanotto, and S. Agrawal, "Rehabilitation exoskeleton design: Exploring the effect of the anterior lunge degree of freedom," *IEEE Trans. Robot.*, vol. 29, no. 4, pp. 838–846, Aug. 2013.
[19] S. Srivastava, P. Kao, S. Kim, P. Stegall, D. Zanotto, J. Higginson, S. Agrawal, and J. Scholz, "Assist-as-needed robot-aided gait training improves walking function in individuals following stroke," *IEEE Trans. Neural Syst. Rehabil. Eng.*, online available.
[20] E. Colgate and N. Hogan, "An analysis of contact instability in terms of passive physical equivalents," in *Proc. IEEE Int. Conf. Robot. Autom.*, 1989, pp. 404–409.
[21] S. Buerger and N. Hogan, "Relaxing passivity for human-robot interaction," in *Proc. IEEE/RSJ Int. Conf. Intell. Robots Syst.*, 2006, pp. 4570–4575.
[22] C. D. Mah, M. Hulliger, R. G. Lee, and I. S. O'Callaghan, "Quantitative analysis of human movement synergies: Constructive pattern analysis for gait," *J. Motor Behav.*, vol. 26, no. 2, pp. 83–102, 1994.
[23] M. W. Spong, S. Hutchinson, and M. Vidyasagar, *Robot Modeling and Control*. New York, NY, USA: Wiley, 2006.
[24] K. K. Patterson, W. H. Gage, D. Brooks, S. E. Black, and W. E. McIlroy, "Evaluation of gait symmetry after stroke: A comparison of current methods and recommendations for standardization," *Gait Posture*, vol. 31, no. 2, pp. 241–246, Feb. 2010.
[25] D. Grieve, "Gait patterns and the speed of walking," *Biomed. Eng.*, vol. 3, no. 3, pp. 119–122, 1968.
[26] S. A. Gard and D. S. Childress, "The influence of stance-phase knee flexion on the vertical displacement of the trunk during normal walking," *Arch. Phys. Med. Rehabil.*, vol. 80, no. 1, pp. 26–32, 1999.
[27] T. Royer and P. Martin, "Manipulations of leg mass and moment of inertia: Effects on energy cost of walking," *Med. Sci. Sport Exerc.*, vol. 37, no. 4, pp. 649–656, 2005.
[28] J. Noble and S. Prentice, "Adaptation to unilateral change in lower limb mechanical properties during human walking," *Exp. Brain Res.*, vol. 169, no. 4, pp. 482–495, 2006.
[29] J. H. Meuleman, E. H. Van Asseldonk, and H. Van der Kooij, "The effect of directional inertias added to pelvis and ankle on gait," *J. Neuroeng. Rehabil.*, vol. 10, no. 40, pp. 1–12, 2013.
[30] E. Van Asseldonk, J. Veneman, R. Ekkelenkamp, J. Buurke, F. Van der Helm, and H. van der Kooij, "The effects on kinematics and muscle activity of walking in a robotic gait trainer during zero-force control," *IEEE Trans. Neural Syst. Rehabil. Eng.*, vol. 16, no. 4, pp. 360–370, Aug. 2008.
[31] J. Kim, D. Oh, S. Kim, and J. Choi, "Visual and kinesthetic locomotor imagery training integrated with auditory step rhythm for walking performance of patients with chronic stroke," *Clin. Rehabil.*, vol. 25, no. 2, pp. 134–145, 2011.
[32] *Safety of Machinery—General Principles for Design—Risk Assessment and Risk Reduction*, International Organization for Standardization, Standard ISO 12100:2010, 2010.
[33] J. F. Veneman, R. Kruidhof, E. E. Hekman, R. Ekkelenkamp, E. H. Van Asseldonk, and H. Van Der Kooij, "Design and evaluation of the LOPES exoskeleton robot for interactive gait rehabilitation," *IEEE Trans. Neural Syst. Rehabil. Eng.*, vol. 15, no. 3, pp. 379–386, Sep. 2007.
[34] S. K. Banala, S. H. Kim, S. K. Agrawal, and J. P. Scholz, "Robot assisted gait training with active leg exoskeleton (alex)," *IEEE Trans. Neural Syst. Rehabil. Eng.*, vol. 17, no. 1, pp. 2–8, Feb. 2009.
[35] D. Zanotto, P. Stegall, and S. K. Agrawal, "Adaptive assist-as-needed controller to improve gait symmetry in robot-assisted gait training," in *Proc. IEEE Int. Conf. Robot. Autom.*, 2014, pp. 724–729.
[36] S. Fisher, L. Lucas, and T. A. Thrasher, "Robot-assisted gait training for patients with hemiparesis due to stroke," *Topics Stroke Rehabil.*, vol. 18, no. 3, pp. 269–276, 2011.

Damiano Zanotto (M'12) received the B.S. *(cum laude)* and M.S. *(cum laude)* degrees in 2005 and 2007, respectively, both in mechanical engineering, and the Ph.D. degree in mechatronics in 2011, all from University of Padua, Padova, Italy.

Between 2011 and 2013, he was a Postdoctoral Fellow with University of Delaware, Newark, DE, USA. He is currently an ARS with Columbia University, New York, NY, USA, where he works on rehabilitation robotics, cable-driven robots, and wearable technology.

Yasuhiro Akiyama received the B.E. degree in engineering from Tokyo Institute of Technology, Tokyo, Japan, in 2006, and the M.S. and Ph.D. degrees in engineering from University of Tokyo, Tokyo, in 2008 and 2011, respectively.

Since 2011, he has been a Postdoctoral Researcher with Nagoya University, Nagoya, Japan. His research interests include mechanical safety, human–robot interaction, and manned space missions.

Paul Stegall (S'10) received the B.S. degree in mechanical engineering from The Johns Hopkins University, Baltimore, MD, USA, in 2009. He is currently working toward the Ph.D. degree in mechanical engineering at Columbia University, New York, NY, USA.

His research interests include robotic rehabilitation, human learning, and gait training.

Sunil K. Agrawal (M'92) received the Ph.D. degree in mechanical engineering from Stanford University, Stanford, CA, USA, in 1990.

He is a Professor with the Department of Mechanical Engineering, Columbia University, New York, NY, USA. He has authored more than 350 journal and conference papers and two books in the areas of controlled mechanical systems, dynamic optimization, and robotics.

Dr. Agrawal received the Presidential Faculty Fellowship from the White House, a Bessel Prize in Germany, and a Humboldt U.S. Senior Scientist Award. He is a Fellow of the ASME and he has been an editorial board member of ASME and IEEE journals.